Low temperature hot filament chemical vapor deposition of Ultrananocrystalline Diamond films with tunable sheet resistance for electronic power devices

J.J. Alcantar-Peña [a,b], J. Montes [b,e], M.J. Arellano-Jimenez [c], J.E. Ortega Aguilar [c], D. Berman-Mendoza [a], R. García [a], M.J. Yacaman [c], O. Auciello [b,d],*

[a] Departamento de Investigación en Física, Universidad de Sonora, Hermosillo, Sonora 83000, Mexico
[b] Materials Science and Engineering, University of Texas-Dallas, Richardson, TX 75080, USA
[c] Physics and Astronomy, University of Texas-San Antonio, San Antonio, TX 78249, USA
[d] Bioengineering, University of Texas at Dallas, Richardson, TX 75080, USA
[e] Departamento de Física, Universidad de Sonora, Hermosillo, Sonora 83000, Mexico

ARTICLE INFO

ABSTRACT

This paper describes the results from systematic experiments performed to investigate the influence of different substrate-filaments distances, surface-substrate temperatures and reaction of precursors during the growth of Ultrananocrystalline Diamond (UNCD) films via the hot filament chemical vapor deposition (HFCVD) process. The experimental results provide valuable information to understand the important role of key molecules (CH_x, x = 1, 2, 3) and atoms (H), resulting from the cracking of precursor molecules (CH_4, H_2) on the hot surface of the filaments, and the contribution of argon (Ar) inert gas atoms, all interacting on the surface of the substrates when using different filaments-substrate distances to produce films with different structures and properties. The interaction of the cracked molecular and atomic species at different filaments-substrate distances, play a critical role in the nucleation and growth of films with different structures, as observed by complementary analytical techniques. Films grown at 5, 15, and 30 mm filaments-substrate distances exhibit graphite-disordered graphene phases, while those grown at 20 mm distances exhibit mixed large UNCD-minor graphite mixed phases, and those grown at 25 and 35 mm distances exhibit pure UNCD phase. UNCD films grown at ~600 °C exhibit grain boundaries with sp^2 and Trans-Polyacetylene (T-PA) dangling chemical bonds and low sheet resistance (~5 Ω), while UNCD films grown at relativity low temperature (~490 °C) exhibit high sheet resistance (~8 MΩ) and more T-PA dangling bonds. The results presented in this paper indicate that UNCD and mixed UNCD/disordered graphene/graphite films can be grown with tailored resistivity enabling potential applications in electronic power devices.

1. Introduction

Diamond films have been attracting the interest of the research and technology-oriented communities because they exhibit a unique combination of properties such as high wear resistance, highest hardness relative to any other film, lowest friction coefficient compared with metal and ceramic coatings, chemical inertness, excellent thermal conductivity (~1500 W/K·m, close to that of single crystal diamond ~2100 W/K·m) perpendicular to the film surface and in the film plane for microcrystalline diamond (≥1 μm grain size), tunable electronic properties by doping, and biocompatible properties. Extensive fundamental and applied science on UNCD films growth has resulted in applications to diverse range of devices [1–4].

Microwave plasma chemical vapor deposition (MPCVD) [1] and hot filament chemical vapor deposition (HFCVD) [5–7] are the two techniques being most used to grow diamond films with various microstructures [1,5–7] and at different substrate temperatures [1,5–7]. UNCD films exhibit high electrical conductivity with either nitrogen incorporated in grain boundaries or boron doping via substitution of B for C atoms in the diamond lattice [1]. Furthermore, UNCD films also exhibits outstanding biocompatibility [1,8–10]. All the UNCD film properties mentioned above enable a broad range of applications to a new generation of mechanical, electronic, energy generation and bio-medical devices.

One topic that has been substantially explored is the UNCD film growth mechanism both for the MPCVD and HFCVD processes. For the HFCVD process, there are various issues that are still under discussion, such as, precursor's reaction at different traveling distance from the

* Corresponding author at: Materials Science & Engineering and Bioengineering, University of Texas-Dallas, 800 W Campbell Rd, Richardson, TX 75080, USA.
E-mail address: orlando.auciello@utdallas.edu (O. Auciello).

moment of their cracking at the hot filaments' surface until the arrival on the substrate's surface to nucleate and induce the growth of the films. The understanding of precursor's reaction during the pathway from the filament towards the substrate surface may be critical to understand the range of carbon faces observed in the films, like disordered graphite/graphene mixtures and UNCD phases with mixtures of sp^2 and T-PA C-atoms bonding in the films' grain boundaries. The precursor's reaction may contribute to tailor chemical bonds and resistivity of UNCD films. The demonstration of the feasibility of growing UNCD films at relativity low (~270 °C [6], 490 °C [7]) or higher (~600 °C) temperatures, with high and low resistivity, respectively, provides the pathway for application to the development of diamond-based devices with tailored resistivity. The feasibility of tuning the chemical bonds of carbon atoms in the grain boundaries of diamond films provides a pathway to the development of diamond-based electronic power devices. One relevant characteristic of polycrystalline diamond films for electronic device applications may be their hydrogenated 2D surface conductivity, which may be provided by chemical dangling bonds on the surface [11–13]. In this respect, by changing the filament-substrate distance, it may be possible to change the nature of the chemical bonds on the surface and grain boundaries of the UNCD films, thus affecting their electrical resistivity, which can provide a pathway for application of UNCD films to the fabrication of diamond-based power devices.

2. Experimental

Because of substrates exchange insertion into the HFCVD film growth chamber, through a load lock, it is not practical to place a thermocouple on the substrate surface every time. Thus, the substrate surface temperature cannot be measured directly during every single film growth. Therefore, a substrate surface temperature calibration was performed before film growth. The temperature calibration was performed using a K-type thermocouple in direct contact with the substrate's surface to measure the substrate surface temperature while exposing it to identical conditions as during film growth. A typical calibration curve correlating the substrate surface temperature and sample holder temperatures applying power in the heater device with filaments off is shown in Fig. 1a. In addition, Fig. 1b shows the calibrated substrate surface temperature for all filament-substrate distances and with filaments on (2200 °C), used for growing all carbon-based films investigated. Fig. 1c shows the temperature distribution in the space between the filaments and the substrates for the different substrate-filaments distance used to grow the films, calculated using the COMSOL 4.2 software. This temperature distribution is critically related to the substrate surface temperature achieved at the different filament-substrate surface distance used to grow all the films described in this paper.

The HFCVD system (Bluewave) features and arrangement of 8 parallel and two angled tungsten (W) filaments (ø = 0.25 mm, length ~ 14.2 cm) (Fig. 2b) held on a molybdenum (Mo) frame positioned above the substrate holder (Fig. 2a and c). The distance between the filaments and the substrate surface was changed by moving the substrate using a motorized Z-driving system (Fig. 2a) provided by the HFCVD manufacturer. The filaments-substrate distances used in the experiments described here were 5, 15, 20, 25, 30 and 35 mm.

The substrates were heated by radiation from the filament plus extra heating provided by heating the substrate heater to 400 °C and 450 °C, as measured by the thermocouple in contact with the heater surface. The substrates were continuously rotated during film growth to provide a uniform temperature and carbon radical species homogeneous distribution on the substrate surface. All films were grown for 2 h. for each experiment, in order to have the time parameter constant for all films. Computer simulations were performed, using a COMSOL 4.2 software, to analyze the temperature distribution in the space between the filaments and the substrates for the different substrate-filaments distance used to grow the films (Fig. 1c).

The filaments were heated to 2200 °C by passing a DC current during the film growth. Films were grown using gas flows of H_2 (5 sccm), CH_4 (1 sccm) and Ar (45 sccm). More details of the UNCD film growth process can be found in our prior paper [7]. The surface morphology, films thickness and nanostructure were characterized using scanning electron microscopy (SEM, ZEISS SUPRA-40) and high-resolution transmission electron microscopy (HRTEM, JEOL 2010F). The samples for the HRTEM analysis were prepared using a focused ion beam (ZEISS FIB-SEM CROSSBEAM) process. The crystallinity and grain sizes of UNCD films were investigated via complimentary HRTEM with electron–diffraction and X-ray diffraction (XRD, Rigaku Ultima III, Cu $K\alpha$ radiation, 1.542 Å). The type of carbon chemical bonding in the films were analyzed via visible Raman spectroscopy, using a Thermo DXR Raman spectrometer with 532 nm wavelength laser beam. The sheet resistance of the UNCD films was measured using an Alessi 4-point probe system with C4S probe head with 1 mm spacing between the tips.

3. Results and discussion

Success in producing continuous and dense UNCD or mixed UNCD-graphite or UNCD-graphite/disordered graphene films at different temperatures, with tailored chemical bonds in grain boundaries and tunable sheet resistance, has important implications for application of these films in electronic power devices like Thin Film Transistors (TFTs) or Schottky diodes, based on nanocarbon films with hydrogenated surface. Fig. 3 shows Raman analysis (using visible 532 nm laser wavelength at
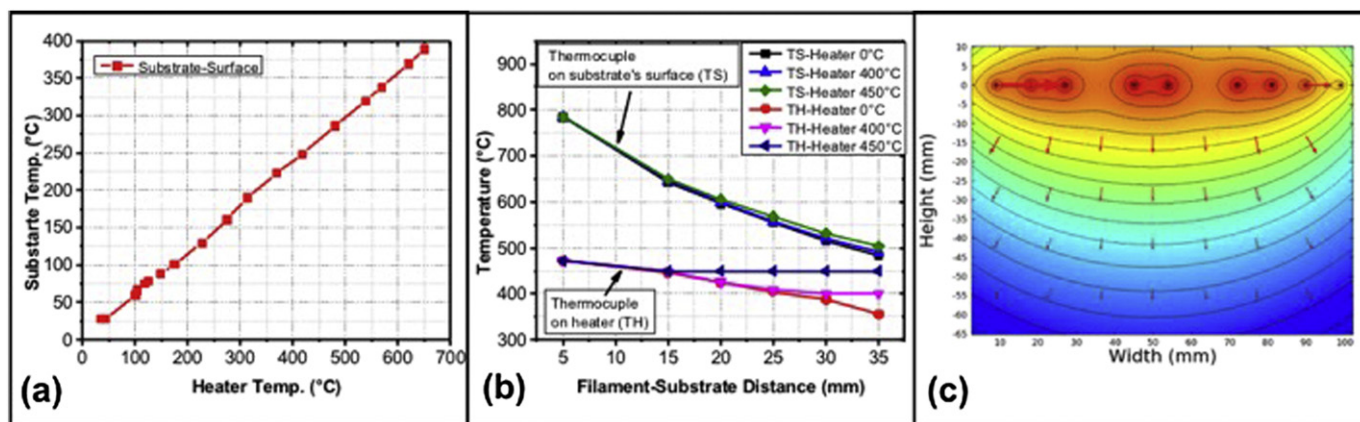

Fig. 1. a) Curve corresponding to the surface-substrate temperature calibration performed to determine the substrate surface temperature during film growth, from reading the temperature provided by the substrate surface-connected thermocouple and the substrate holder-connected thermocouple; b) substrate surface temperature vs. filament-substrate distance; c) temperature distribution in the space between the filaments and the substrates for the different substrate-filaments distance used to grow the UNCD films, calculated using the COMSOL 4.2 software.
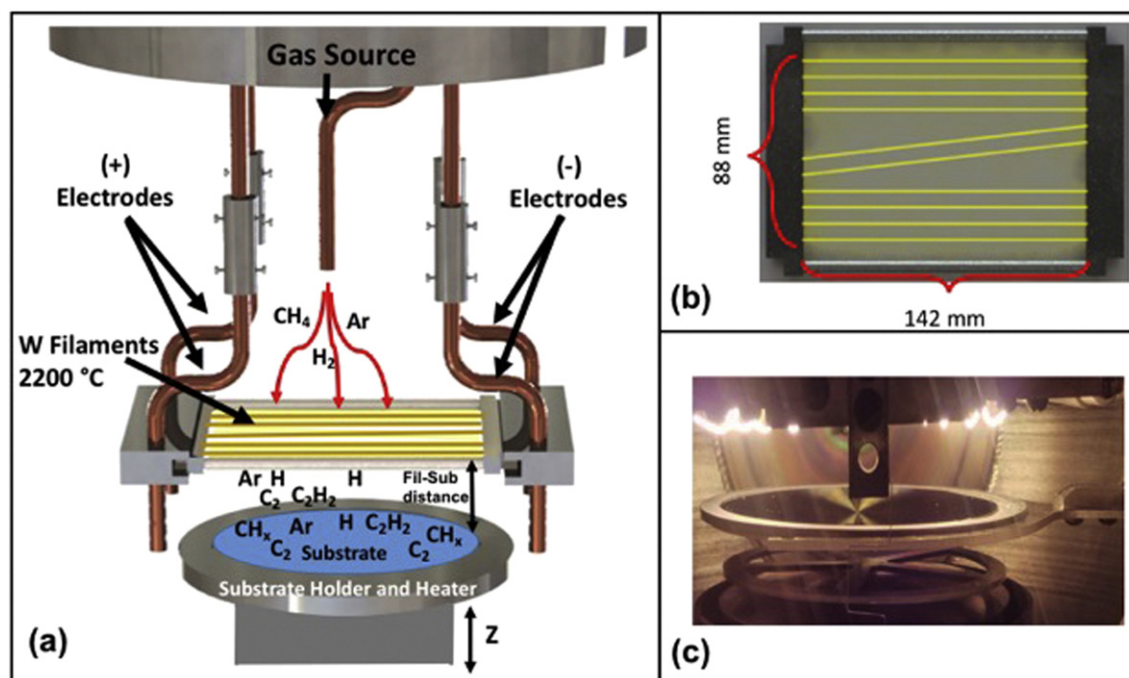
Fig. 2. a) Schematic of the HFCVD-substrate geometrical arrangement and gas flow and species involved in the UNCD film growth process via the HFCVD system used in the experimental work described here; b) schematic of the filament arrangement (the specific filament arrangement shown in the figure is the one that provides the best film thickness uniformity in conjunction with the appropriate filament-substrate distances of 25, 30, and 35 mm (see Table 1), across 100 mm diameter substrates, compared with UNCD films grown with other filament arrangements); c) picture of the HFCVD system at the time of transferring a substrate into the growth chamber from the load-lock (the rotating holder on which the substrate holder is positioned can be seen under the substrate holder with the wafer).

1 mW of power) of films grown at substrate surface temperatures in the range 490–800 °C for filament-substrate distances of 5 mm to 35 mm (Fig. 3a and b). The temperature of the substrate surface was reached by the addition of the filament radiation at different filament-substrate distances plus additional heating from the holder heater to 400 °C (Fig. 3a) and 450 °C (Fig. 3b). It is important to emphasize that all films, for which Raman analyses are shown in Fig. 3, were grown at different substrate-filaments distances, as indicated in that figure.

The contributions of the heat supplied by the filament radiation, the substrate positions, the heat supplied by the substrate holder heater and the reaction of the precursors at different traveling distance from the moment of precursor's cracking at the hot filaments surface, until the

nucleation and film growth on the substrate surface, can be seen from the Raman analysis. The spectra show characteristic D band (~1340 cm^{-1}) and G band (~1588 cm^{-1}), peaks 5 and 3, respectively, from the sp^2 C-atoms bond hybridization. Deconvolution of the Raman peaks (not shown to simplify the spectrum figure) of the UNCD films shows that there is a contribution of three extra peaks between 1000 and 2000 cm^{-1}, peak 4 (~1489 cm^{-1}), peak 6 (~1258 cm^{-1}) and peak 7 (~1164 cm^{-1}), to the D and G peaks, reported as representative of C$=$C stretching of Trans-PolyAcetillene (T-PA), broadened vibrational density of states (VDOS) of small diamond clusters, and tetrahedral amorphous carbon, and T-PA C—H bending combined with C—C stretching, respectively. [14–17] In addition, the wavenumber range of
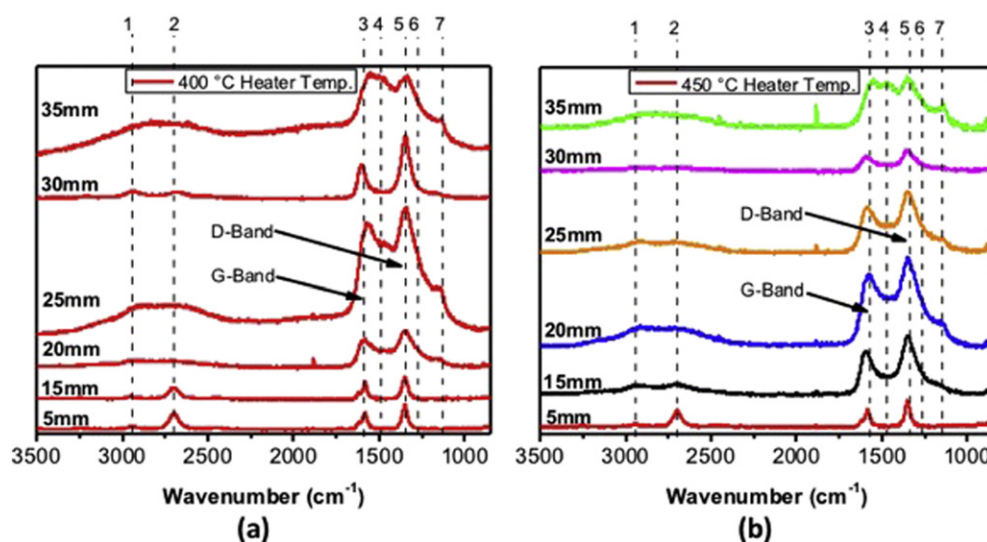
Fig. 3. Raman spectra of films grown at filament-substrate distances from 5 mm to 35 mm with the substrate heater heated to 400 °C (a) and 450 °C (b), respectively, read by the thermocouple in contact with the substrate holder surface.

3500–2500 cm^{-1} include peaks 1 (~2947 cm^{-1}) and 2 (~2700 cm^{-1}), which are D + G-mode and 2D-mode respectively.

At the nearest substrate-filaments distance (5 mm), and due to the high filament radiation heating, the films are grown with the substrate surface at ≥800 °C. The films grown at this high temperature show Raman peaks characteristic of structural disordered graphene (2D (2700 cm^{-1}) and D (1340 cm^{-1}) band peaks), with the graphene structure, seen also in other HFCVD growth [18], confirmed by HRTEM (not shown). The results described above on change of the diamond phase to graphite or disordered graphene, are in agreement with prior studies, which showed that the diamond structure is damaged or changed into other carbon structures other than diamond when it is exposed to high temperatures (≥800 °C) [19,20]. Raman analysis revealed structural changes in the films grown at 15–35 mm filament-substrate distances when supplying heat to the substrate surface from the substrate heater, in addition to the heating supplied by the filament radiation (Fig. 3a–b). Specifically, for films grown at 5 and 15 mm filament-substrate distance, mainly a structural disordered graphene was observed, as revealed by Raman analysis for the film grown with substrate holder heater heated to 400 °C (confirmation by HRTEM-not shown), and a mixture of graphite and UNCD was detected for the films grown with the substrate heater heated to 450 °C (substrate surface at ~650 °C-see Fig. 3b, with confirmation by HRTEM-Fig. 4a). The conclusions presented above, from the Raman analysis, are based on the observation of the high intensity and shape of the characteristic D band (1340 cm^{-1}) and G band (1588 cm^{-1}) peaks from the sp^2 hybridization, and very low signal from the three extra peaks at 1489 cm^{-1}, 1258 cm^{-1} and 1164 cm^{-1} known as C≡C stretching of Trans-PolyAcetillene (T-PA), broadened vibrational density of states (VDOS) of small diamond clusters and tetrahedral amorphous carbon, and T-PA C—H bonding combined with C—C stretching, respectively [14–16,

20]. For films grown at 20 and 25 mm filament-substrate distance, the characteristic visible Raman spectrum of UNCD films was observed for films grown with the substrate holder heater set up at 400 °C and 450 °C, respectively (Fig. 3a–b, confirmed by HRTEM-Fig. 4b–c). At 30 mm filament-substrate distance, the films showed a graphitic phase mixed with UNCD for films grown both with theater set up at 400 °C and 450 °C (Fig. 3a–b, confirmed by XRD analysis). Finally, films grown at 35 mm filament-substrate distance with similar heater and substrate surface temperature as for the case of film grown at 30 mm filament-substrate distance, exhibit the characteristic UNCD structure, as revealed by visible Raman analysis (Fig. 3a–b, confirmed by HRTEM-Fig. 4d).

The UNCD films grown at 35 mm filament-substrate distance exhibit an intense signal from T-PA dangling bonds at grain boundaries and particularity they were produced at relativity low substrate surface temperature (~490 °C), increasing the substrate compatibility. Similar UNCD films grown at about 500 °C on Si substrates were observed by X. Xiao et al. [2], using the MPCVD process. The heat transfer simulation by COMSOL at different substrate-filaments distances, shown in Fig. 1c, indicate that at close distance (0–15 mm height) to the filaments, the temperature radiation it's mainly driven by the number and position of the filaments, and the temperature fluctuations correlate with the film thickness fluctuations shown in Table 1.

The structures of key films were analyzed by HRTEM, as shown in Fig. 4, for films grown at 15 mm (a), 20 mm (b), 25 mm (c) and 35 mm (d) filament-substrate distance at 450 °C heater temperature for all films. The diffraction patterns show diffraction rings related to Van der Waals and covalent bond distance corresponding to the graphite structure in the mixed graphite-UNCD film structure in Fig. 4a, and the diffraction peaks and rings corresponding to the (111) and (220) diamond planes in Fig. 4a and the UNCD films in Figs. 4b–d. The
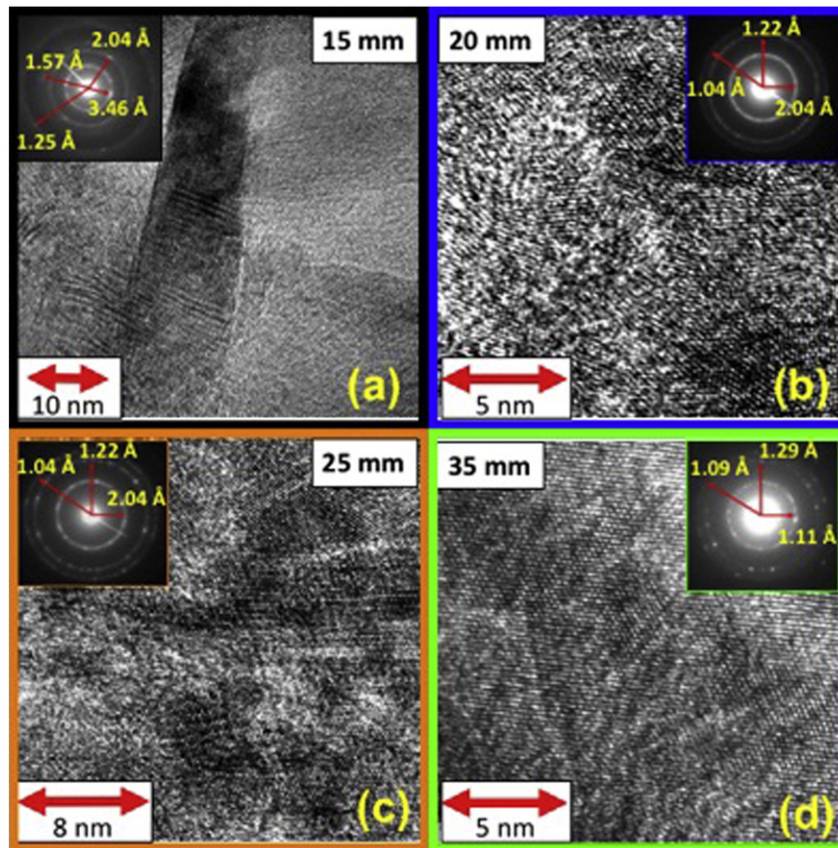
Fig. 4. HRTEM images from films grown at different filament-substrate distance and 450 °C heater temperature: (a) 15 mm (large graphite-small UNCD mixture), (b) 20 mm, (c) 25 mm, (d) 35 mm (UNCD films), correlating with Raman spectra shown in Fig. 3b (match the frame colors in this figure with the spectra color in Fig. 3b).

Table 1

UNCD film thickness as obtained from SEM cross section measurements at different positions across the films on 100 mm diameter substrates for films grown with different substrate temperatures and different substrate-filaments distances. The better uniformity observed for UNCD films grown at 25, 30, and 35 mm filament-substrate distance correlates with the better heat distribution across the filaments length as revealed by the calculations shown in Fig. 1c.

Distance (mm)	Thickness (nm) Heater at 400 °C Center | Middle | Edge	Thickness (nm) Heater at 450 °C Center| Middle| Edge
5	989.2 – 1209 – 565.2	1512.3 – 1227.3 – 1686.3
15	322.7 – 334.2 – 134.0	325 – 325.4 – 240.4
20	177.9 – 147.7 – 76.61	419.1 – 386.8 – 245.1
25	277.2 – 248.0 – 76.6	171.5 – 154.2 – 114.2
30	239.2 – 221.5 – 154.2	251.7 – 220.3 – 180.2
35	81.4 – 81.8 – 54.6	137.0 – 118.5 – 78.3

crystallinity characteristic of the diamond phase in the UNCD films, determined by electron diffraction patterns, was confirmed by XRD analysis (see Fig. 6 and Table 2).

Fig. 5 shows top view SEM pictures of the morphologies of thin films grown at different filament-substrate distances and substrate temperatures, namely: (a) films grown with heater at 400 °C and (b) heater at 450 °C. The characteristics of the films are explained in the figure caption.

Table 1 shows all the film thickness measurements from SEM cross sections (not shown) obtained at different wafer positions for films grown with different heater temperatures (substrate surface temperatures) and different substrate-filaments distances. The larger film thickness variations across the film surface, observed for films grown at 5 and 15 mm filament-substrate distance, are mainly driven by the number and position of the filaments at closer distances due to thermal radiation effects as described above (see Fig. 1c).

The importance of performing analysis with complimentary techniques is revealed by the fact that in the electron diffraction analysis of the films grown at 15 mm filament-substrate distance (Fig. 4a) the evidence of the existence of a minor diamond phase mixed with the major graphitic phase observed is confirmed in the XRD analysis of the same film. The XRD analysis for a film grown at 5 and 15 mm filament-substrate distance shows a major peak (1 at 26.54°) corresponding to the graphitic (002) phase (black and red spectrums - Fig. 6) and also small peaks (4 at ~44.01°, corresponding to diamond (111), 7 at 75.44°, corresponding to diamond (220) and 8 at 91.70°, corresponding

Table 2

Diffraction angles, lattice spacing, grain size and lattice constant from films grown a 5 mm, 15 mm, 20 mm, 25 mm, 30 mm and 35 mm filament-substrate distances at 450 °C heater temperature.

Distance (mm)	Position (°2θ)	Miller indices (hkl)	d-Spacing d (A)	Grain size (nm)	Lattice constant (A)	Material
5	26.25	002	3.3923	5.64	6.7845	Graphite
15	26.54	002	3.3558	6.55	6.7117	Graphite
30	26.33	002	3.3821	4.77	6.7643	Graphite
5	43.25	111	2.0902	3.43	3.6204	Diamond
15	43.38	111	2.0842	3.06	3.6101	Diamond
20	44.01	111	2.0559	4.36	3.5609	Diamond
25	44.08	111	2.0527	4.30	3.5556	Diamond
30	43.73	111	2.0684	3.81	3.5826	Diamond
35	44.17	111	2.0488	6.78	3.5487	Diamond
5	75.03	220	1.2649	6.86	3.5777	Diamond
15	74.94	220	1.2662	7.87	3.5814	Diamond
20	75.34	220	1.2605	4.85	3.5652	Diamond
25	75.18	220	1.2628	4.50	3.5716	Diamond
30	75.02	220	1.2651	5.65	3.5781	Diamond
35	75.44	220	1.2589	5.62	3.5607	Diamond
20	91.70	311	1.0728	4.60	3.5582	Diamond
25	92.09	311	1.0701	13.08	3.5487	Diamond
35	91.79	311	1.0727	10.09	3.5579	Diamond

to diamond (311)). These diamond peaks are the dominant peaks in the XRD spectra of the UNCD films grown at 20 (blue curve), 25 (brown curve), and 35 (violet curve) mm filament-substrate distance (Fig. 6). For the case of 30 mm (green curve), a balanced mixture of graphite and UNCD phases was observed. The XRD analysis shows excellent agreement with the HRTEM images and electron diffraction analysis shown in Fig. 4b–d and the Raman analysis of the same films shown in Fig. 3a–b. In addition to the XRD peaks corresponding to the graphitic and diamond phases, peaks 2 and 3 at 34.76° and 39.51, respectively, correspond to tungsten carbide from the interface between the UNCD film and the tungsten layer on the Si substrate on which the UNCD films were grown on the carbide nucleation layer. Finally, the peaks 5 and 6 at 54.45° and 61.80° correspond to Tungsten from the tungsten layer grown on the Si substrate.

Diffraction angles, lattice spacing, grain size and lattice constant from films grown at 5 mm, 15 mm, 20 mm, 25 mm, 30 mm and 35 mm at 450 °C heater temperature substrate surface temperature are summarized in Table 2.

The observed variations in the diamond lattice d-spacing correspond to residual stress on the films. The XRD analysis shows that the d-spacing in the diamond lattice, calculated from Bragg's law, is decreasing from 2.0559 Å for the film grown at 20 mm filament-substrate distance to 2.0488 Å for the film grown at 35 mm filament-substrate distance, which relates to a reduction of the lattice constant from 3.5609 Å to 3.5487 Å, thus revealing that the UNCD films are under compressive stress [17,21]. The comparison of the XRD and HRTEM analysis of the films grown at 15 mm filament-substrate distance shows excellent agreement in confirming that the films structure correspond to a diamond phase immersed in a graphitic matrix, which is the dominant material phase in the films.

Fig. 7 shows the sheet resistance of films grown at different heater temperature/substrate surface temperature and substrate-filaments distances.

The data presented above provides good information showing the dominant high resistivity diamond phase in the UNCD films grown at 25 and 35 mm filament-substrate distance and 400 °C heater temperature, and the low resistivity mixed graphite-diamond phase in the films grown at 15, 20 and 30 mm filament-substrate distance and 450 °C heater temperature. However, in order to understand how the structural phase-change in the films affect the electrical conductivity, four points probe measurements were performed. These measurements were focused on measuring the sheet resistance only, since it is very well know that electrical conductivity through UNCD films is controlled extensively by the grain boundaries [22,23], due to dangling bonds, and over the surface by quantum states of holes accumulated on the 2D surface layer formed on hydrogenated air-exposed top-surface region of diamond [11,12]. By comparing the sheet resistance results with the Raman analysis, it can be seen that those films that have low sheet resistance (mΩ to Ω) correspond to those featuring the graphite phase only or UNCD films with sp^2 hybridization bonds in the grain boundaries (confirmed by HRTEM analysis). On the other hand, films with high sheet resistance (kΩ to MΩ) correspond to those with more T-PA and more organized structure between grain boundaries (see HRTEM results). Therefore, it is relevant to optimize the structure of the UNCD films, in terms of graphite-diamond phases, which according to the results presented above can be achieved by optimizing the filament-substrate distance and the substrate surface temperature. The experimental evidence shown in this paper, indicates that being able to change the sheet resistance of the UNCD films may provide the bases for application of these films to Schottky and/or Thin Film Transistor devices, since hydrogenated bulk diamond and polycrystalline diamond (MCD) have been used as active layer for those kind of devices [24–27]. The current problem with yet non-optimized UNCD films relates to the low surface resistance (mΩ), while all the devices such as FETs and MISFET that have been fabricated with hydrogenated surface exhibit resistance in the order of (kΩ–MΩ). However, it is expected that the sheet resistance
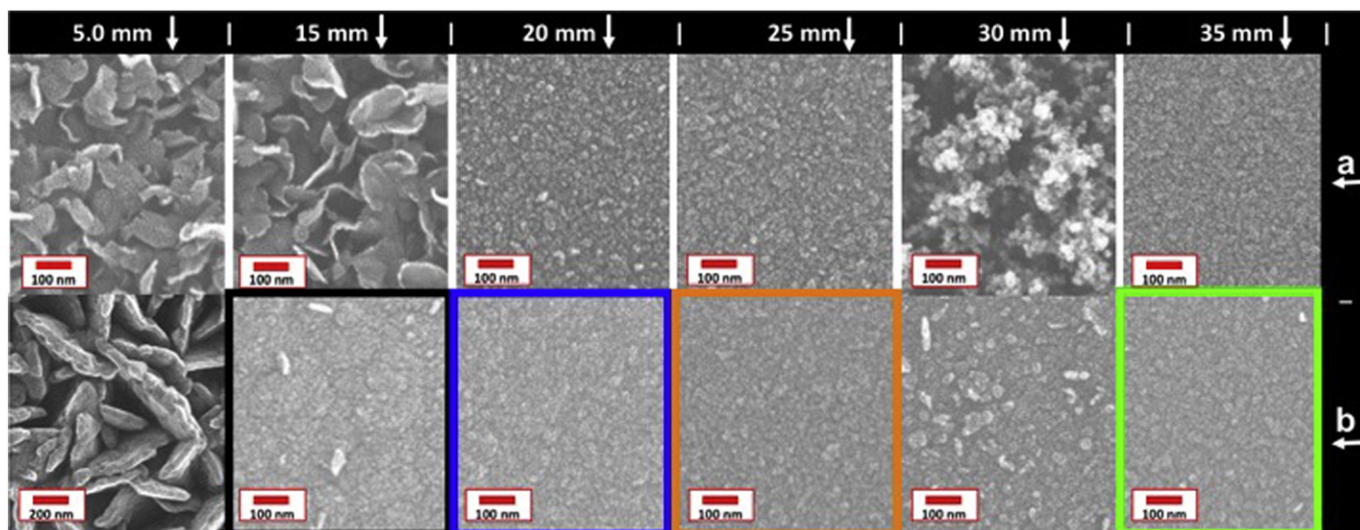
Fig. 5. SEM top view images of the films grown at different filament-substrate distances and substrate surface temperatures: a) films grown with the heater at 400 °C and b) with the heater at 450 °C. The SEM pictures of the surface of the films grown at 20, 25, and 35 mm filament-substrate distance for both substrate heater heated to 400 °C and 450 °C show the topography characterized by the nanostructure of UNCD films; the SEM pictures of films grown at 5, 15, and 30 mm filament-substrate distances with the heater at 400 °C and 5 mm with the heater at 450 °C show the characteristic surface morphology of graphite; the films grown at 15 and 30 mm filament-substrate distances with the heater at 450 °C show a surface morphology of mixed UNCD-graphite phases (match the frame colors in this figure with the spectra color in Fig. 3b).

of the UNCD films can be increased by tailoring the grain boundaries chemical bonds, as a promising option, which is currently being explored.

4. Conclusions

Systematic studies were performed to investigate the effect of different substrate-filaments distance, substrate surface temperature and precursor's reactions in the space between filaments and substrate, during the growth of Ultrananocrystalline Diamond (UNCD) films using the HFCVD process. Analysis of the grown films, using complementary (Raman, HRTEM, SEM and XRD) characterization techniques and

sheet resistance measurements, revealed the important role played by C-based precursor's reaction at different traveling distance from the moment of being cracked on the surface of the hot filaments until nucleation on the substrate surface to produce films with different structures, including structural disordered graphene, UNCD-Graphite mixture or single phase UNCD. Films grown at 5 mm filament-substrate distance show graphite and structural disordered graphene phases. Films grown at 15 and 30 mm filament-substrate distance show UNCD embedded in a graphite matrix structure, and films grown at 20, 25 and 35 mm filament-substrate distance show the characteristic UNCD structure, and grain boundaries with sp^2 and T-PA chemical bonds configurations, respectively. Films with grain boundaries featuring mainly sp^2 chemical bonds exhibit low sheet resistance (mΩ–Ω), while films featuring mainly T-PA bonded boundaries show high sheet resistance (kΩ–MΩ). The finding that UNCD films can also be grown at relatively low temperature (~490 °C), using an Ar/CH$_4$/H$_2$ gas mixture and without using unconventional gases such as H$_2$S used in the past [6] to grow diamond films at low temperature by HFCVD, correlates with prior demonstration that UNCD films can be grown at temperatures in
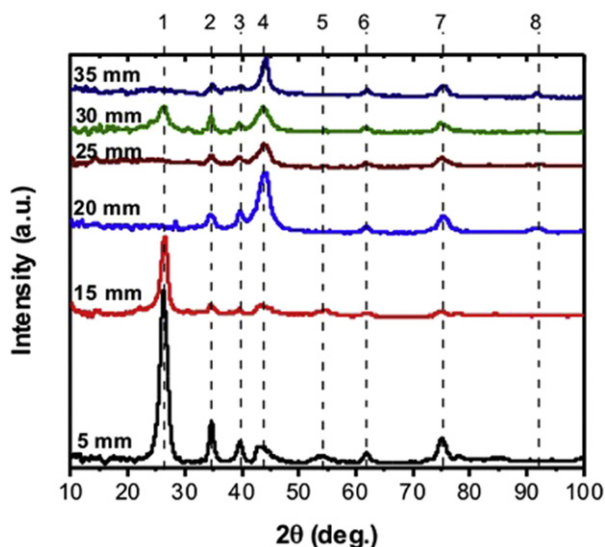

Fig. 6. XRD spectra from analysis of films grown at 5 mm, 15 mm, 20 mm, 25 mm, 30 mm and 35 mm filament-substrate distance at 450 °C heater temperature. The black and red spectra show the dominant graphite peak (1) and very small diamond peaks (4, 7, and 8) for the film grown at 5 and 15 mm filament-substrate distance. The blue, brown and violet spectra show the dominant diamond peaks (4, 7, and 8) characteristic of high quality UNCD films; the green spectra shows a balanced mixture of graphite and UNCD phases.
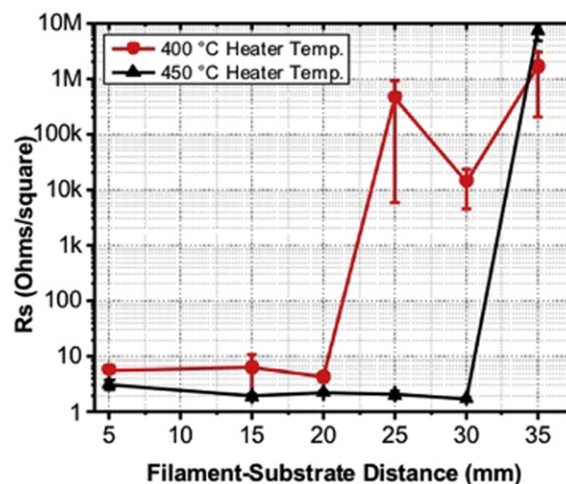

Fig. 7. Sheet resistance of UNCD films grown at 400 and 450 °C heater temperature at different filaments-substrate distance.

the range 350–400 °C via the MPCVD process [1], and has important implications for HFCVD growth of UNCD films for application to fabrication of Thin Film Transistors (TFTs) or Schottky diodes with hydrogenated surface for electronic power devices.

Acknowledgments

References

[1] O. Auciello, A.V. Sumant, Status review of the science and technology of ultrananocrystalline diamond (UNCD™) films and application to multifunctional devices, Diam. Relat. Mater. 19 (7–9) (2010) 699.

[2] X. Xiao, J. Birrell, J.E. Gerbi, O. Auciello, J.A. Carlisle, Low temperature growth of ultrananocrystalline diamond, J. Appl. Phys. 96 (4) (2004) 2232.

[3] A.R. Krauss, O. Auciello, D.M. Gruen, A. Jayatissa, A. Sumant, J. Tucek, D. Mancini, N. Moldovan, A. Erdemir, D. Ersoy, M.N. Gardos, H.G. Busmann, E.M. Meyer, M.Q. Ding, Ultrananocrystalline diamond thin films for MEMS and moving mechanical assembly device, Diam. Relat. Mater. 10 (11) (2001) 1952.

[4] O. Auciello, J. Birrell, J.A. Carlisle, J.E. Gerbi, X. Xiao, B. Peng, H.D. Espinosa, Materials science and fabrication processes for a new MEMS technology based on ultrananocrystalline diamond thin films, J. Phys. Condens. Matter 16 (16) (2004) R539.

[5] J. Zimmer, K.V. Ravi, Aspect of scaling CVD diamond reactors, Diam. Relat. Mater. 15 (2006) 229.

[6] F. Piazza, G. Morell, Synthesis of diamond at sub 300 °C substrate temperature, Diam. Relat. Mater. 16, (2007) (1950).

[7] E.M.A. Fuentes-Fernandez, J.J. Alcantar-Peña, G. Lee, A. Boulom, H. Phan, B. Smith, T. Nguyen, S. Sahoo, F. Ruiz-Zepeda, M.J. Arellano-Jimenez, P. Gurman, C.A. Martinez-Perez, M.J. Yacaman, R.S. Katiyar, O. Auciello, Synthesis and characterization of microcrystalline diamond to ultrananocrystalline diamond films via hot filament chemical vapor deposition for scaling to large area applications, Thin Solid Films 603 (2016) 62.

[8] X. Xiao, J. Wang, J.A. Carlisle, B. Mech, R. Greenberg, R. Freda, M.S. Humayun, J. Weiland, O. Auciello, In vitro and in vivo evaluation of ultrananocrystalline diamond for coating of implantable retinal microchips, J. Biomed. Mater. Res. B Appl. Biomater. 77 (2) (2006) 273–281.

[9] O. Auciello, P. Gurman, M.B. Guglielmotti, D.G. Olmedo, A. Berra, M.J. Saravia, Bio-compatible ultrananocrystalline diamond coatings for implantable medical devices, MRS Bull. 39 (07) (2014) 621.

[10] P. Bajaj, D. Akin, A. Gupta, D. Sherman, B. Shi, O. Auciello, R. Bashir, Ultrananocrystalline diamond film as an optimal cell interface for biomedical applications, Biomed. Microdevices 9 (6) (2007) 787.

[11] L. Gan, E. Baskin, C. Saguy, R. Kalish, Quantization of 2D hole gas in conductive hydrogenated diamond surfaces observed by electron field emission, Phys. Rev. Lett. 96 (19) (2006) 196808.

[12] C.E. Nebel, B. Rezek, A. Zrenner, Electronic properties of the 2D-hole accumulation layer on hydrogen terminated diamond, Diam. Relat. Mater. 13 (11 − 12) (2004) 2031.

[13] L. Gan, C. Saguy, E. Baskin, R. Kalish, Electron field emission from the 2D hole gas in hydrogen terminated, polycrystalline diamond, Diam. Relat. Mater. 17 (3) (2008) 336.

[14] V.I. Merkulov, J.S. Lannin, C.H. Munro, S.A. Asher, V.S. Veerasamy, W.I. Milne, UV studies of tetrahedral bonding in diamondlike amorphous carbon, Phys. Rev. Lett. 78 (25) (1997) 4869.

[15] J. Robertson, E.P. O'Reilly, Electronic and atomic structure of amorphous carbon, Phys. Rev. B 35 (6) (1987) 2946.

[16] F. Klauser, D. Steinmüller-Nethl, R. Kaindl, E. Bertel, N. Memmel, Raman studies of nano- and ultra-nanocrystalline diamond films grown by hot-filament CVD, Chem. Vap. Depos. 16 (4–6) (2010) 127.

[17] A.C. Ferrari, J. Robertson, Interpretation of Raman spectra of disordered and amorphous carbon, Phys. Rev. B 61 (20) (2000) 14095.

[18] F. Mendoza, T.B. Limbu, B.R. Weiner, G. Morell, Large-area bilayer graphene synthesis in the hot filament chemical vapor deposition reactor, Diam. Relat. Mater. 51 (2015) 34.

[19] B.V. Deryagin, D.V. Fedosayev, Special issue on diamond growth and films. the growth of diamond and graphite from the gas phase, Surf. Coat. Technol. 38 (1) (1989) 131.

[20] T. Evans, P.F. James, A study of the transformation of diamond to graphite, Proc. R. Soc. Lond. A Math. Phys. Eng. Sci. 277 (1369) (1964) 260.

[21] Y. Fu, H. Du, C.Q. Sun, Interfacal structure, residual stress and adhesion of diamond coatings deposited on titanium, Thin Solid Films 424 (1) (2003) 107.

[22] L. Wang, Q. Zeng, J. Huang, R. Xu, K. Tang, J. Zhang, Y. Xia, Influence of the diamond grain size on the electrical properties of nano-crystalline diamond film detectors, Thin Solid Films 520 (2) (2011) 717.

[23] L. Gan, A. Bolker, C. Saguy, R. Kalish, D.L. Tan, B.K. Tay, D. Gruen, P. Bruno, The effect of grain boundaries and adsorbates on the electrical properties of hydrogenated ultra nano crystalline diamond, Diam. Relat. Mater. 18 (9) (2009) 1118.

[24] J.W. Liu, M.Y. Liao, M. Imura, E. Watanabe, H. Oosato, Y. Koide, Diamond logic inverter with enhancement-mode metal-insulator-semiconductor field effect transistor, Appl. Phys. Lett. 105 (8) (2014) 082110.

[25] J.C. Madaleno, S.C. Trippe, L. Pereira, Comparison of the electrical behavior of Schottky diodes built on the nucleation and growth surfaces of polycrystalline diamond, Diam. Relat. Mater. 16 (4–7) (2007) 926.

[26] H. Kozak, A. Kromka, O. Babchenko, B. Rezek, Directly grown nanocrystalline diamond field-effect transistor microstructures, Sens. Lett. 8 (3) (2010) 482.

[27] O.A. Williams, Ultrananocrystalline diamond for electronic applications, Semicond. Sci. Technol. 21 (8) (2006) R49.